



HAL
open science

Topographical and nanomechanical characterization of casein nanogel particles using atomic force microscopy

Asma Bahri, Marta Martin, Csilla Gergely, Sylvie Marchesseau, Dominique Chevalier-Lucia

► **To cite this version:**

Asma Bahri, Marta Martin, Csilla Gergely, Sylvie Marchesseau, Dominique Chevalier-Lucia. Topographical and nanomechanical characterization of casein nanogel particles using atomic force microscopy. *Food Hydrocolloids*, 2018, 83, pp.53-60. 10.1016/j.foodhyd.2018.03.029 . hal-01793780

HAL Id: hal-01793780

<https://hal.science/hal-01793780>

Submitted on 26 May 2020

HAL is a multi-disciplinary open access archive for the deposit and dissemination of scientific research documents, whether they are published or not. The documents may come from teaching and research institutions in France or abroad, or from public or private research centers.

L'archive ouverte pluridisciplinaire **HAL**, est destinée au dépôt et à la diffusion de documents scientifiques de niveau recherche, publiés ou non, émanant des établissements d'enseignement et de recherche français ou étrangers, des laboratoires publics ou privés.

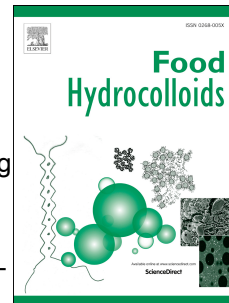


Distributed under a Creative Commons Attribution 4.0 International License

Accepted Manuscript

Topographical and nanomechanical characterization of casein nanogel particles using atomic force microscopy

Asma Bahri, Marta Martin, Csilla Gergely, Sylvie Marchesseau, Dominique Chevalier-Lucia



PII: S0268-005X(17)32061-1

DOI: [10.1016/j.foodhyd.2018.03.029](https://doi.org/10.1016/j.foodhyd.2018.03.029)

Reference: FOOHYD 4340

To appear in: *Food Hydrocolloids*

Received Date: 13 December 2017

Revised Date: 14 March 2018

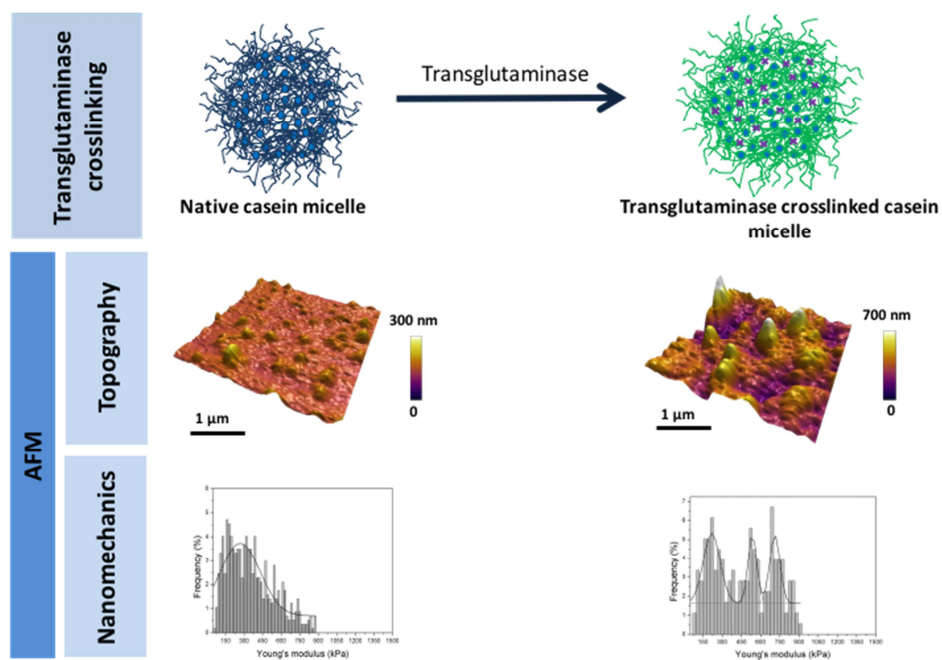
Accepted Date: 14 March 2018

Please cite this article as: Bahri, A., Martin, M., Gergely, C., Marchesseau, S., Chevalier-Lucia, D., Topographical and nanomechanical characterization of casein nanogel particles using atomic force microscopy, *Food Hydrocolloids* (2018), doi: 10.1016/j.foodhyd.2018.03.029.

This is a PDF file of an unedited manuscript that has been accepted for publication. As a service to our customers we are providing this early version of the manuscript. The manuscript will undergo copyediting, typesetting, and review of the resulting proof before it is published in its final form. Please note that during the production process errors may be discovered which could affect the content, and all legal disclaimers that apply to the journal pertain.

Comment citer ce document :

Bahri, A., Martin, M., Gergely, C., Marchesseau, S., Chevalier-Lucia, D. (2018). Topographical and nanomechanical characterization of casein nanogel particles using atomic force microscopy. *Food Hydrocolloids*, 83, 53-60. , DOI : 10.1016/j.foodhyd.2018.03.029



Comment citer ce document :

Bahri, A., Martin, M., Gergely, Marchesseau, S., Chevalier-Lucia, D. (2018). Topographical and nanomechanical characterization of casein nanogel particles using atomic force microscopy. Food Hydrocolloids, 83, 53-60. , DOI : 10.1016/j.foodhyd.2018.03.029

1 **Topographical and nanomechanical characterization of casein nanogel** 2 **particles using atomic force microscopy**

3

4 Asma Bahri^a, Marta Martin^b, Csilla Gergely^b, Sylvie Marchesseau^a, Dominique Chevalier-
5 Lucia^{a*}

6 ^a IATE, Université de Montpellier, CIRAD, INRA, Montpellier SupAgro, Montpellier,
7 France

8 ^b L2C, Université de Montpellier, CNRS, Montpellier, France

9 *Corresponding author:

10 dominique.chevalier-lucia@umontpellier.fr

11 Université de Montpellier

12 CC023 – UMR IATE

13 Place Eugène Bataillon

14 34095 Montpellier cedex 5 - France

15

16 **Abstract**

17 Casein micelle (CM), porous colloidal phosphoprotein-mineral complex, naturally present in
18 milk to deliver minerals, also has several features, which could ensure its use as nanocarrier
19 for bioactives. CM structure being not steady according to the physico-chemical conditions,
20 its stability can be improved by intra-micellar cross-linking using transglutaminase (TGase)
21 inducing a strengthened structure called casein nanogel. The aim of this research was to
22 investigate the morphology and nanomechanics of casein nanogel particles cross-linked by
23 TGase (TG-CM) using atomic force microscopy (AFM) in native-like liquid environment
24 (lactose-free simulated milk ultrafiltrate, SMUF). Prior to AFM, TG-CM were captured by
25 anti-phospho-Ser/Thr/Tyr monoclonal antibodies covalently bound to a gold-coated slide via

26 carbodiimide chemistry. Surface topography and size properties evaluation revealed an
27 increase in size of TG-CM compared to native CM, TG-CM being characterized by a mean
28 width of 264 ± 7 nm and a mean height of 111 ± 5 nm. TG-CM displayed a relatively high
29 contact angle (62°) indicating a limited flattening of these particles after adsorption on the
30 substrate. The TG-CM elasticity was then evaluated applying low indentation forces on single
31 TG-CM. The TGase treatment led to a significant modification of CM nanomechanics
32 attributed to intramolecular rearrangements within the micellar structure. The elasticity
33 distribution of TG-CM revealed three elasticity peaks centered at 219 ± 14 kPa, 536 ± 14 kPa
34 and 711 ± 11 kPa. The lower elasticity peak is related to the native CM elasticity
35 characteristic and the two stiffer peaks were attributed to the substantial changes in the TG-
36 CM structure.

37

38 **Keywords:** Casein micelle; Nanogel; Transglutaminase; Atomic force microscopy;
39 Topography; Nanomechanics

40

41 1. Introduction

42 With the growing awareness of food importance on disease prevention and cure, novel
43 strategies have been developed to include and deliver bioactive compounds through food
44 matrices (Katouzian & Jaffary, 2016; Prakash & van Boekel, 2010; Zhu, 2017). Particularly,
45 nanoencapsulation of bioactives has been proposed to protect them against degradation during
46 processing, increase their bioavailability and monitor their release to the desired site after
47 ingestion (Katouzian & Jaffary, 2016). Casein micelles (CM) are natural polymeric
48 nanocarriers for delivery of minerals, particularly calcium and phosphate (de Kruif & Holt,
49 2003). Consequently, bioactives delivery systems have been developed from nanosized native
50 CM or modified CM (Chevalier-Lucia, Blayo, Gracià-Julià, Picart-Palmade, & Dumay, 2011;
51 Livney, 2010; Ranadheera, Liyanaarachchi, Chandrapala, Dissanayake, & Vasiljevic, 2016).
52 CM is a naturally self-assembly of caseins, major milk proteins (~ 80%), through
53 hydrophobic bonds and colloidal calcium phosphate bridges. The main four caseins α_{s1} , α_{s2} , β
54 and κ are phosphoproteins present at a molar ratio of ~4:1:4:1.6 in CM (Walstra, Geurts,
55 Noomen, Jellema, & van Boekel, 1999). CM has a hydrodynamic diameter of ~200 nm and a
56 highly hydrated structure retaining ~3.7 g water/g of dry casein (McMahon & Brown, 1984).
57 It is characterized by a hydrophobic core and a hydrophilic shell, CM surface being covered
58 by a κ -casein brush insuring its stability thanks to electrostatic and steric repulsion (Dalglish,
59 Horne, & Law, 1989; De Kruif & Zhulina, 1996; Horne, 2006). Moreover, the porous and
60 open structure of CM due to the high proline content provides an excellent release mechanism
61 for bioactive delivery in the stomach (Fox, 2003; Livney, 2010). Consequently, CM can be an
62 excellent matrix to carry hydrophobic molecules and other biopolymers (Ranadheera et al.,
63 2016). Caseins without a well-defined permanent second or tertiary structure have been
64 described as rheomorphic (Holt & Sawyer, 1993) meaning that they may adapt their structure
65 to suit various conditions. CM structure is therefore not steady since several structural

66 modifications can occur and even lead to the disruption of the CM framework due to changes
67 of physico-chemical parameters such as pH, ionic strength, water activity, temperature or
68 pressure (De La Fuente, 1998; Gaucheron, 2005). However, CM structural stability can be
69 improved by intra-micellar cross-linking using transglutaminase enzyme (TGase) to form
70 strengthened structures called casein nanogel particles (De Kruif, Huppertz, Urban, &
71 Petukhov, 2012; Huppertz & de Kruif, 2008; Smiddy, Martin, Kelly, de Kruif, & Huppertz,
72 2006).

73 TGase has several applications in food processing aiming to enhance functional properties of
74 proteins (Romeih & Walker, 2017; Yokoyama, Nio, & Kikuchi, 2004) by catalyzing covalent
75 binding between protein-bound glutaminy side chain and protein-bound lysyl side chain
76 (Motoki, Seguro, Nio, & Takinami, 1986). It has been clearly shown that TGase cross-linking
77 increases the stability of CM against dissociating agents (Smiddy et al., 2006), ethanol
78 coagulation (Huppertz & De Kruif, 2007a) and heat treatment (O'Sullivan, Kelly, & Fox,
79 2002). Particularly, many studies have focused on the major gel property modifications
80 obtained from TGase cross-linked CM (Ardelean, Jaros, & Rohm, 2013; Jaros, Jacob, Otto, &
81 Rohm, 2010; Lorenzen, Neve, Mautner, & Schlimme, 2002). However, up to now, the
82 topographical and nanomechanical properties of individual TG-CM have never been
83 investigated.

84 The aim of the present research is to evaluate the morphology and nanomechanics of TGase
85 cross-linked CM (TG-CM) using atomic force microscopy (AFM) in lactose-free simulated
86 milk ultrafiltrate (SMUF, pH 6.6) to replicate the native mineral environment of CM (Jenness
87 & Koops, 1962). This technique provides soft material evaluation with minimal sample
88 preparation to preserve its native properties (Jiao & Scha, 2004; Kasas, Longo, & Dietler,
89 2013). Nevertheless, AFM requires the immobilization of samples on a flat surface prior to
90 study. In this work, CM and TG-CM were captured before AFM by weak interactions via a

91 specific MAH-PSer/Thr/Tyr antibody covalently bound to a carboxylic acid self-assembled
92 monolayer on a gold surface. This capture method was previously developed and tested on
93 native casein micelles (Bahri et al., 2017). The characterization of TG-CM, individual internal
94 cross-linked casein micelle, was carried out in parallel with that of native CM and was also
95 intended to validate the sensitivity of this methodology to investigate the topographical and
96 nanomechanical properties of casein micelles.

97

98 **2. Material and methods**

99 **2.1. Reagents**

100 Tri-potassium citrate, tri-sodium citrate, KH_2PO_4 , K_2SO_4 were purchased from Alfa Aesar
101 (Heysham, UK). K_2CO_3 and CaCl_2 were from Amresco (Solon, Ohio, USA) and acetic acid,
102 MgCl_2 , KCl and KOH from VWR BDH Prolabo (Fontenay-sous-bois, France). 11-mercapto-
103 1-undecanoic acid (11-MUA), N-ethyl-dimethylaminopropylcarbodiimide (EDC), N-
104 hydroxysuccinimide (NHS) and sodium azide were obtained from Sigma-Aldrich (Saint-
105 Quentin Fallavier, France). Sodium acetate was purchased from Merck (Darmstadt,
106 Germany). Transglutaminase (TGase, Activa WM®) was a gift from Ajinomoto Foods
107 Europe S.A.S. (Mesnil-Saint-Nicaise, France). Mouse anti-human phospho-Ser/Thr/Tyr
108 monoclonal antibody (MAH-PSer/Thr/Tyr antibody) was from Spring Bioscience (E3074 -
109 Pleasanton, CA, USA). HBS-N buffer (0.01 M HEPES, 0.15 M NaCl, pH 7.4) and
110 ethanolamine hydrochloride 1 M pH 8.5 were purchased from Biacore (GE Healthcare,
111 Velizy-Villacoublay, France). All solutions were prepared using Milli-Q water (Millipore®).

112

113 **2.2. Preparation of native and cross-linked casein micelle dispersions**

114 Native phosphocasein (PC) powder purchased from Ingredia SA (Promilk 852B, lot 131088,
115 Arras, France) has been industrially obtained by microfiltration and diafiltration using the

116 milk mineral soluble phase ensuring a quasi-native state to the prepared casein micelles. PC
117 powder contained 95 g dry solids per 100 g of powder and, in dry basis (w/w), 86% total
118 proteins (corresponding to 79.1% caseins).

119 Casein micelle dispersion (5%, w/w) was prepared by dissolving PC powder in pH 6.6
120 lactose-free simulated milk ultrafiltrate (SMUF), replicating the mineral environment of
121 native CM (Jenness & Koops, 1962). The dispersion was stirred at 540 rpm for 30 min at 20
122 °C before being stored overnight at 4 °C improving powder hydration. The PC dispersion was
123 then warmed at 40 °C for 1 h and rapidly cooled to 20 °C just before experiments to ensure
124 complete equilibration. To prevent microbial growth, sodium azide (0.35 g/L) was added to
125 all samples.

126 CM cross-linked by TGase (TG-CM) were obtained from PC dispersion prepared as
127 described above, equilibrated at 30 °C for 2 h and then incubated with 0.5 g/L TGase (100
128 U/g activity) at 30 °C for 24 h. Then, TGase was inactivated by heating the dispersion at 70
129 °C for 10 min, followed by a rapid cooling to room temperature in an ice-water bath (Smiddy
130 et al., 2006). The cross-linkage of CM by TGase was checked by investigating the CM
131 demineralization by sodium citrate addition up to 100 mmol.L⁻¹ and turbidity measurements at
132 633 nm (Huppertz, Smiddy, & de Kruif, 2007) as shown in Table S1. A PC control dispersion
133 was concurrently prepared following the same thermal history as TG-CM but without
134 addition of TGase.

135

136 **2.3. Micelle size distribution by photon correlation spectroscopy**

137 The CM size distribution was evaluated by photon correlation spectroscopy (PCS) using a
138 Zetasizer Nano-ZS equipment (Malvern Instruments, Malvern, UK) at 25 °C. Before
139 analyses, each sample was diluted 20-fold with SMUF to avoid multiple diffusion phenomena
140 during PCS measurement. Experimental data were assessed by the NNLS algorithm with the

141 dispersant viscosity taken as 0.89 mPa.s and the refractive index as 1.33 at 25 °C.
142 Characteristics of the dispersed CM particles were taken as for milk proteins: 0.004 and 1.36
143 for the imaginary and the real refractive indices, respectively (Regnault, Thiebaud, Dumay, &
144 Cheftel, 2004). For each independent sample, a mean distribution curve in intensity and in
145 number was calculated from six measurements as well as the mean diameter (arithmetical
146 mean).

147

148 **2.4. Scanning electron microscopy (SEM)**

149 Scanning electron microscopy (SEM) was used to evaluate CM shape. SEM samples were
150 prepared as described in a previous work (Gastaldi, Lagaude, & De La Fuente, 1996). Briefly,
151 ANODISC® membranes (Whatman, Maidstone, England) with an average pore diameter of
152 200 nm were immersed overnight in CM dispersion. After dehydration in a series of graded
153 ethanol solutions (25-100%), the specimens were dried using a critical point dryer (Bal-Tec
154 AG, Balzers, Liechtenstein, Germany). Then, the patterns were sputtered with gold palladium
155 and analyzed with a Hitachi S-4800 scanning electron microscope at an accelerating voltage
156 of 2 kV.

157

158 **2.5. Atomic force microscopy**

159 **2.5.1. CM capture for AFM experiment**

160 CM were captured by low energy interactions via MAH-PSer/Thr/Tyr antibody as described
161 in a previous work (Bahri et al., 2017). All immobilization steps were carried out at room
162 temperature. As a first step, a gold-sputtered glass chip (AU.0500.ALSI, Platypus
163 Technologies LLC, Madison, WI, USA) was chemically cleaned twice with piranha solution
164 (70% H₂SO₄ plus 30% H₂O₂), then three times with ethanol. The cleaned chip was
165 immediately immersed in an ethanolic solution of 11-MUA (5 mM) for 18 h to coat the

166 surface with a self-assembled monolayer (SAM) of carboxyl groups. The chip was then
167 extensively rinsed with absolute ethanol and ultrapure water before being immersed for 1 h in
168 a MAH-PSer/Thr/Tyr antibody solution (50 $\mu\text{g/mL}$) prepared in acetate buffer (10 mM, pH
169 5). It was rinsed with acetate buffer (10 mM, pH 5), then with HBS-N buffer (0.01 M HEPES,
170 0.15 M NaCl, pH 7.4) before immersion into ethanolamine solution (1 M, pH 8) for 30 min to
171 block free binding sites. The prepared chip was then immediately immersed into the TG-CM
172 dispersion for 1 h, rinsed with SMUF and equilibrated for 4 h at room temperature before
173 AFM measurements.

174 2.5.2. AFM measurements

175 The AFM experimental system used was an Asylum MFP-3D head coupled to the Molecular
176 Force Probe 3D controller (Asylum Research, Santa Barbara, CA, USA). The microscope was
177 placed in an acoustic isolation enclosure with an anti-vibration system. Silicon nitride
178 cantilevers MLCT were purchased from Veeco Metrology Group (Santa Barbara, CA, USA),
179 with a nominal spring constant of 0.01 N.m^{-1} and an half-opening angle of 35° . Prior to each
180 experiment, the cantilever spring constant was determined in liquid environment using the
181 thermal noise method included in the MFP-3D software. AFM height, deflection trace and
182 retrace topographic images, with a pixel resolution of 256 pixels at a line rate of 0.6 Hz, were
183 obtained in contact mode in SMUF at room temperature. After testing a range of loading
184 forces on different individual TG-CM, measurements were performed with a maximum
185 loading force of $\sim 100 \text{ pN}$. Higher loading force values led to stiffness overestimation due to
186 the substrate. It was particularly checked that CM and TG-CM retained the same spherical
187 cap section shape and remained adhered before and after indentation experiments (Figure S1).
188 A constant approach velocity of $6 \mu\text{m.s}^{-1}$ was used, meaning a piezo-extension rate of 3 Hz to
189 minimize hydrodynamic and viscoelastic artifacts (Rosenbluth, Lam, & Fletcher, 2006).

190 The height (h) and width (w) distributions were obtained from the single TG-CM size
191 analysis using the MFP-3D software. The contact angle (θ) of each TG-CM was deduced
192 from the AFM-measured height and width using the equation (1):

$$193 \quad \theta = 180 \text{ Arccos} (1 - (h/w)) / \pi \quad (1)$$

194 The elastic deformation was obtained from the force curves as a function of the loading force
195 applied by the tip. The Young's modulus (E) was calculated for each force curve from the
196 approaching part of the curve according to a modified Hertz model (Hertz, 1881), as
197 described by Martin et al. (2013).

198 Experiments were repeated 3 times on different AFM gold chips.

199

200 2.5.3. AFM data analysis

201 Raw images were corrected by an implemented Asylum software using a standard procedure
202 (flatten, planefit and artifact lines caused by the tip attachment and removal). Longitudinal
203 profiles at selected zones were also obtained by the software. The scale indicating the sample
204 height or deflection was adjusted to limit the gap between high and low regions. The
205 individual elasticity values for a sample were collected via the Asylum software providing the
206 distribution of elasticity values. Counts were normalized considering the total collected
207 elasticity values of the specimen. A Gaussian fitting was then applied using the multi-peak
208 analyzing software implemented in the MFP-3D operating system and OriginPro 8 software.

209

210 2.6. Statistics

211 Results were expressed as mean \pm standard deviation. All the AFM and PCS results were
212 analyzed by the Student's t-test. Statistical significance was set at $p < 0.05$.

213

214 3. Results and discussion

215 3.1. Topography of transglutamisase cross-linked CM

216 The influence of TG cross-linking has been evaluated on the apparent CM shape and
217 dimensions. Fig. 1a-h shows AFM height and deflection images of CM and TG cross-linked
218 CM captured on SAM-gold substrate via MAH-PSer/Thr/Tyr antibody when imaged in
219 contact mode under native conditions (SMUF, pH 6.6). Scan parameters were adjusted for
220 optimum contrast and stability and no lateral displacement of particles was recorded during
221 analyses. These images (Fig. 1a-h) emphasize the efficiency of specific antibody capture of
222 TG-CM that reveal a spherical cap shape, as already observed for native CM (Bahri et al.,
223 2017). The native CM and TG-CM surface appears topographically homogeneous. This
224 observation was confirmed by SEM micrographs (Fig. 2), which display different-sized CM
225 and TG-CM (range of 40-300 nm) with a typical spherical shape and a rough surface.
226 Moreover, SEM images of TG-CM (Fig. 2b, d) do not show the presence of CM aggregates
227 proving that TGase cross-linking is exclusively intra-micellar.

228 According to the 2D and 3D AFM heights (Fig. 1a, c, e, g, h, j, l), it appeared that TG-CM are
229 higher and wider than native CM. The surface coverage of TG-CM (11 ± 4 micelles/ μm^2) was
230 significantly ($p < 0.05$) lower than the native CM surface coverage (20 ± 2 micelles/ μm^2), this
231 lower density being attributed to the smaller size of native CM compared to TG-CM. At the
232 same time, the hydrodynamic diameter distribution curves of native CM and TG-CM
233 measured by PCS have been compared. The both size distribution curves in intensity exhibit
234 monomodal and polydisperse populations (Fig. 3). TG-CM have however a significantly ($p <$
235 0.05) higher average hydrodynamic diameter of 214 ± 8 nm compared to 192 ± 8 nm for
236 native CM.

237 This result was confirmed by the height and width distributions (Fig. 4a, b) obtained from the
238 single TG-CM size analysis using the MFP-3D software. All in all, 250 features obtained
239 from 10 different 2D-AFM images were analyzed. The size counts were normalized

240 considering the total collected values of samples. A multi-peak fitting was then applied using
241 OriginPro 8 software to calculate the mean width and height. As depicted in Fig. 4a, b, TG-
242 CM are polydisperse with monomodal width and height distributions and they are
243 significantly ($p < 0.05$) wider (264 ± 7 nm) and higher (111 ± 5 nm) than native CM
244 investigated in the same conditions and characterized by a mean width of 148 ± 8 nm and a
245 mean height of 42 ± 1 nm (Bahri et al., 2017).

246 The morphological AFM results as those from SEM strongly show that TGase cross-linking is
247 intra- and not inter-micellar, which is in good agreement with previous studies that underlined
248 the intra-micellar cross-linking of native CM using different methods such as PCS, SLS and
249 SAXS (Huppertz & De Kruif, 2008). However, it has been until now mentioned that CM size
250 was not modified by TGase cross-linking. Nevertheless, the present results obtained from
251 AFM and PCS data indicate that TGase cross-linking increases CM size as also observed
252 previously on covalently cross-linked CM using genipin (Nogueira Silva, Bahri, Guyomarc'h,
253 Beaucher, & Gaucheron, 2015). On the other hand, from SEM images (Fig. 2), the size
254 difference between native CM and TG-CM was not clearly observable. This phenomenon
255 could be attributed to CM shrinkage caused by the critical point drying of samples during the
256 preparation steps since CM are highly hydrated features and therefore, drying process has an
257 important impact on micellar structure. These observations are in accordance with other
258 studies reporting distortion of CM particles due to the drying step during sample preparation
259 for SEM (Dalglish, Spagnuolo, & Goff, 2004; Martin, Goff, Smith, & Dalglish, 2006;
260 McMahon & Oommen, 2008).

261 AFM size characteristics were used to calculate the native CM and TG-CM volume; it should
262 remain constant even after particle adsorption upon the surface (Evangelopoulos, Glynos, &
263 Koutsos, 2012). The volume of the TG-CM was then calculated using MFP-3D software by
264 performing the sum of all the heights of the micelle multiplied by the X scale and Y scale.

265 TG-CM have a volume of $\sim 5 \times 10^6 \text{ nm}^3$ that higher than that measured for native CM ($\sim 1 \times$
266 10^6 nm^3), leading to a mean diameter of 214 nm for TG-CM and 123 nm for native CM
267 considering CM as spherical. These values are consistent with the hydrodynamic diameter
268 obtained by PCS for TG-CM.

269 Height and width distributions (Fig. 4a, b) show that TG-CM captured on SAM-gold substrate
270 via MAH-PSer/Thr/Tyr antibody were definitely larger than higher, as it was also the case for
271 native CM (Bahri et al., 2017). According to AFM size data, native CM and TG-CM have the
272 shape of a spherical cap section rather than a sphere. This deformation, attributed to the
273 adsorption upon gold substrate, can be evaluated by the ratio calculation between height and
274 width, the perfect spherical particle width being equal to its height ($h/w \sim 1$). TG-CM data
275 reveal a h/w ratio of ~ 0.5 higher than the native CM ratio (~ 0.3), indicating that native CM
276 have a flatter shape compared to TG-CM. A previous study also evaluated the h/w ratio equal
277 to 0.3 for native CM in liquid conditions and also highlighted CM deformation due to
278 attachment on the substrate without losing volume in the case of CM immobilization on gold
279 substrate via amine-coupling strategy (Ouanezar, Guyomarc'h, & Bouchoux, 2012). The h/w
280 ratio of native CM and TG-CM implies a liquid droplet like behavior (Helstad et al., 2007).
281 This deformation can also be displayed by plotting the height against the width for each single
282 object (Fig. 4c, d). The comparison with the dotted line representing a perfect sphere points
283 towards the fact that the TG-CM (Fig. 4c) are less flattened compared to native CM (Fig. 4d)
284 once captured on the gold substrate. This phenomenon clearly highlights a structural
285 strengthening of CM due to the molecular rearrangements induced by TGase.

286 The CM contact angle was deduced from the AFM-measured (h and w) of each CM. The
287 contact angle (θ) corresponding to the interior angle formed by the substrate and the tangent
288 to the drop interface at the apparent intersection of these interfaces describes the object
289 deformation upon adsorption (Brown, 1999; Russel, 2009). A small contact angle is observed

290 when the particle spreads on the surface, while a large contact angle is observed when the
291 liquid beads on the surface. More specifically, a perfect spherical particle would exhibit a
292 contact angle greater than 90° (Yuehua & Randall, 2013). The equilibrium shape of a given
293 particle does not depend only on surface forces but is also greatly affected by the elastic
294 modulus of the droplet, the droplet deformation depending of material elastic nature resulting
295 from stress development across the bulk in opposition to that deformation (Brown, 1999;
296 Evangelopoulos et al., 2012). According to the AFM data analysis, TG-CM have a contact
297 angle θ of 62° against the coated surface. Conversely, native CM have a significantly ($p <$
298 0.05) lower contact angle value of 44° . These results confirm the observed less deformation
299 of TG-CM than native CM after capture on gold substrate.

300 An important change of the CM topography and elastic properties occurred after CM cross-
301 linking with TGase compared to native CM. Cross-linked CM were significantly higher and
302 larger than native CM pointing towards significant modifications in the CM structure due to
303 TG crosslinking. A previous study highlighted a similar effect on CM height after
304 crosslinking with genipin by AFM measurements in air, but widths were narrower probably
305 due to dry condition (Nogueira Silva et al., 2015). Unlike control native CM, TG-CM were
306 less deformed when adsorbed on gold substrate as reflected by a higher contact angle.
307 Depending strongly on object elasticity, this high contact angle value revealed the harder
308 aspect of TG-CM compared to native CM. The ratio h/w confirmed this observation since it
309 was higher than that evaluated for native CM.

310

311 **3.2. Nanomechanical properties of TG-CM**

312 To explore nanomechanical properties of CM, low indenting forces were applied on each
313 individual micellar object. CM kept the same shape and neither displacement nor
314 disintegration was recorded after indentation experiments. A low loading force value of ~ 100

315 pN was chosen for nanoindentation to avoid CM damage due to the AFM tip and ensure a
316 minimal deformation in the CM-substrate region. Ten force curves were applied at the center
317 of each individual CM. The elasticity of CM at a given position was then calculated by fitting
318 the approach part of the force curve using the Hertz model (Hertz, 1881; Uricanu, Duits, &
319 Mellema, 2004) (Figure S2). In order to confirm the position of the analyzed particles,
320 successive images were regularly performed and compared (Figure S1). Furthermore, by
321 reducing the indentation to 20 nm, the contribution of the hard substrate on the calculated
322 elasticity value was minimized. The elasticity of 20 micellar objects was calculated to obtain
323 about 200 elasticity values.

324 The histogram of TG-CM stiffness values (Fig. 5) reveals a multimodal stiffness distribution
325 with three prominent peaks at 218 ± 14 kPa, 536 ± 10 kPa and 711 ± 11 kPa, as identified by
326 the peak analyzing software. The intensity of the three Gaussian distributions used to fit the
327 TG-CM histogram is similar suggesting that the three populations have the same weight (Fig.
328 5). In comparison, a broad unimodal stiffness distribution with a peak centered at 269 ± 14
329 kPa was observed for native immobilized CM (Fig. 5). Generally, the mechanical
330 heterogeneity of apparent Young's moduli is attributed to the complexity of the CM structure,
331 the AFM tip indenting different components of the outer layer or of the core of CM (Bahri et
332 al., 2017). Actually, hydrophobic bonds, negatively charged surface and calcium phosphate
333 nanoclusters are involved in this complexity. In the case of TG-CM, the softest stiffness peak
334 value (218 ± 14 kPa) is comparable to native CM Young's modulus value ($269 \text{ kPa} \pm 14 \text{ kPa}$),
335 and presumably represents a population with characteristics close to those of native CM. The
336 two other stiffer peaks (535 ± 10 kPa and 710 ± 11 kPa) were most likely due to substantial
337 changes in the shape and structure of CM induced by the TGase activity, as suggested by the
338 size and topographical AFM data. This modification could be attributed to the creation of new
339 casein dimers and oligomers formed by crosslinking peptide bound glutamine and lysine

340 residues after incubation with TGase (Ardelean et al., 2013; Smiddy et al., 2006). It is
341 demonstrated that TGase creates intramicellar bonds; hence, κ -casein which is placed on the
342 surface of the CM is the most involved in the polymerization reaction started by TGase
343 followed by β and α_s casein, respectively (Ardelean et al., 2013; Huppertz & de Kruif, 2007a,
344 2007b; Jaros et al., 2010; Sharma, Lorenzen, & Qvist, 2001). This is probably related to the
345 respective locations of caseins within the CM since CM is recognized as complex network of
346 caseins chains with κ -casein hairy layer predominately present on the surface while β -casein
347 is mostly present in the interior and α_s -casein is located all over the structure (Dalglish &
348 Corredig, 2012; De Kruif & Holt, 2003; Marchin, Putaux, Pignon, & Léonil, 2007).

349 To date, there are very few studies in literature on the effect of TGase cross-linking on the
350 elasticity of individual CM at nanoscopic scale. Nieuwland, Bouwman, Bennink, Silletti, &
351 de Jongh (2015) investigated the elastic modulus of individual CM cross-linked by TGase at
352 different concentrations (0 to 90 U/g) using the Derjaguin, Muller, Toporov model applied on
353 AFM force curves. The maximum modulus was observed for the highest TGase
354 concentration, slightly lower than the TGase concentration fixed in this study. This is in
355 accordance with the present results since the stiffness distribution of TG-CM was
356 characterized by two peaks (536 ± 10 kPa and 711 ± 11 kPa) stiffer than the native CM
357 Young's modulus value (269 kPa ± 14 kPa).

358 At macroscopic scale, the cross-linked TG-CM have been investigated focusing on TG-CM
359 gelling properties by rheological measurements, highlighting an increase in stiffness and
360 breaking strain of the TG-CM acid gels (Anema, Lauber, Lee, Henle, & Klostermeyer, 2005;
361 Faergemand & Qvist, 1997; Faergemand, Sorensen, Jorgensen, Budolfsen, & Qvist, 1999;
362 Lauber, Henle, & Klostermeyer, 2000). The gel microstructure modification observed in these
363 studies at the macroscopic scale is attributed to the introduction of new covalent bonds in
364 individual CM. This resulted at nanoscale in a higher stiffness of individual TG-CM

365 compared to native CM as shown by AFM nanomechanical characterization indicating that
366 TGase modified the nanoscale organization of CM from colloids association to microgel
367 particles.

368 Besides, these AFM results on the nano-structural properties of individual CM after
369 enzymatic cross-linking highlight significant modifications probably inducing changes in the
370 functional properties of caseins.

371

372 **Conclusions**

373 In summary, this study of TG-CM by AFM in liquid environment presents the first
374 investigation on the size and nanomechanical properties of individual TG-CM. The AFM 2D
375 images reveal a spherical-cap shape with a wider (264 ± 7 nm) and higher (111 ± 5 nm)
376 structure than native CM. Moreover, TG-CM shows a more resistant structure upon
377 adsorption on gold substrate owing to a high contact angle of 62° .

378 The TG-CM nanomechanical properties highlight a low elasticity peak at 218 ± 14 kPa that
379 could correspond to the mechanical signature of native CM and also two stiffer elasticity
380 peaks observed at 536 ± 10 kPa and 711 ± 11 kPa, most likely directly related to substantial
381 changes in the shape and structure of CM induced by TGase and responsible for the
382 modification of their functional properties.

383 These results support the improved stability of TG-CM suggesting that these nanogel particles
384 can be an excellent matrix for bioactives encapsulation.

385

386 **Acknowledgements**

387 We thank the French Ministry of Higher Education and Research for financial support and M.
388 D. COT from the European Institute of Membrane, Montpellier, France for the SEM analysis.

389 Transglutaminase Activa® WM was kindly provided by Ajinomoto Foods Europe S.A.S
390 (Mesnil-Saint-Nicaise, France).

391

392 **References**

393 Anema, S. G., Lauber, S., Lee, S. K., Henle, T., & Klostermeyer, H. (2005). Rheological
394 properties of acid gels prepared from pressure- and transglutaminase-treated skim milk.

395 *Food Hydrocolloids*, 19(5), 879–887.

396 Ardelean, A. I., Jaros, D., & Rohm, H. (2013). Influence of microbial transglutaminase cross-
397 linking on gelation kinetics and texture of acid gels made from whole goats and cows
398 milk. *Dairy Science and Technology*, 93(1), 63–71.

399 Bahri, A., Martin, M., Gergely, C., Pugnère, M., Chevalier-Lucia, D., & Marchesseau, S.
400 (2017). Atomic force microscopy study of the topography and nanomechanics of casein
401 micelles captured by an antibody. *Langmuir*, 33(19), 4720–4728.

402 Brown, R. (1999). *Handbook of polymer testing* (Marcel Dek). New York.

403 Chevalier-Lucia, D., Blayo, C., Grácia-Juliá, A., Picart-Palmade, L., & Dumay, E. (2011).
404 Processing of phosphocasein dispersions by dynamic high pressure: Effects on the
405 dispersion physico-chemical characteristics and the binding of α -tocopherol acetate to
406 casein micelles. *Innovative Food Science and Emerging Technologies*, 12(4), 416–425.

407 Dalgleish, D. G., & Corredig, M. (2012). The structure of the casein micelle of milk and Its
408 changes during processing. *Annual Review of Food Science and Technology*, 3, 449–467.

409 Dalgleish, D., Horne, D. S., & Law, A. J. R. (1989). Size-related differences in bovine casein
410 micelles. *Biochimica et Biophysica Acta*, 991, 383–387.

411 Dalgleish, D. G., Spagnuolo, P. A., & Goff, H.D. (2004). A possible structure of the casein
412 micelle based on high-resolution field-emission scanning electron microscopy.
413 *International Dairy Journal*, 14, 1025–1031.

- 414 De Kruif, C. G., & Holt, C. (2003). Casein micelle structure, functions and interactions.
415 *Advanced Dairy Chemistry*, 1(3), 233–275.
- 416 De Kruif, C. G., & Zhulina, E. B. (1996). κ -Casein as a polyelectrolyte brush on the surface
417 of casein micelles. *Colloids and Surfaces A: Physicochemical and Engineering Aspects*,
418 117(1–2), 151–159.
- 419 De Kruif, C. G., Huppertz, T., Urban, V. S., & Petukhov, A. V. (2012). Casein micelles and
420 their internal structure. *Advances in Colloid and Interface Science*, 171–172, 36–52.
- 421 De La Fuente, M. A. (1998). Changes in the mineral balance of milk submitted to
422 technological treatments. *Trends in Food Science and Technology*, 9(7), 281–288.
- 423 Evangelopoulos, A. E. A. S., Glynos, E., & Koutsos, V. (2012). Elastic Modulus of a Polymer
424 Nanodroplet : Theory and Experiment. *Langmuir*, 10(28), 4754–4767.
- 425 Faergemand, M., & Qvist, K. B. (1997). Transglutaminase: effect on rheological properties,
426 microstructure and permeability of set style acid skim milk gel. *Food Hydrocolloids*,
427 11(3), 287–292.
- 428 Faergemand, M., Sorensen, M., Jorgensen, U., Budolfsen, G., & Qvist, K. (1999).
429 Transglutaminase: effect on instrumental and sensory texture of set style yoghurt.
430 *Milchwissenschaft-Milk Science International*, 54, 563–566.
- 431 Fox, P. F. (2003). Milk proteins: general and historical aspects. In P. F. Fox & P. L. H.
432 McSweeney (Eds.), *Advanced Dairy Chemistry: volume 1: Proteins, Parts A&B* (pp. 1–
433 48). Springer US.
- 434 Gastaldi, E., Lagaude, A., & De La Fuente, B. T. (1996). Micellar transition state in casein
435 between pH 5.5 and 5.0. *Journal of Food Science*, 61(1), 59–64.
- 436 Gaucheron, F. (2005). The minerals of milk. *Reproduction, Nutrition, Development*, 45, 473–
437 483.
- 438 Helstad, K., Rayner, M., Van Vliet, T., Paulsson, M., & Dejmek, P. (2007). Liquid droplet-

- 439 like behaviour of whole casein aggregates adsorbed on graphite studied by
440 nanoindentation with AFM. *Food Hydrocolloids*, 21(5–6), 726–738.
- 441 Hertz, H. (1881). Über die Berührung fester elastischer Körper. *Journal Für Die Reine Und*
442 *Angewandte Mathematik*, 92, 156–171.
- 443 Holt, C., & Sawyer, L. (1993). Caseins as rheomorphic proteins: interpretation of primary and
444 secondary structures of the α s1-, β - and κ -caseins. *Journal of the Chemical Society,*
445 *Faraday Transactions*, 89(15), 2683–2692.
- 446 Horne, D. S. (2006). Casein micelle structure: Models and muddles. *Current Opinion in*
447 *Colloid & Interface Science*, 11(2–3), 148–153.
- 448 Huppertz, T., & de Kruif, C. G. (2007a). Ethanol stability of casein micelles cross-linked with
449 transglutaminase. *International Dairy Journal*, 17(5), 436–441.
- 450 Huppertz, T., & de Kruif, C. G. (2007b). Rennet-induced coagulation of enzymatically cross-
451 linked casein micelles. *International Dairy Journal*, 17(5), 442–447.
- 452 Huppertz, T., Smiddy, M. A., & de Kruif, C. G. (2007). Biocompatible micro-gel particles
453 from cross-linked casein micelles. *Biomacromolecules*, 8, 1300–1305.
- 454 Huppertz, T., & de Kruif, C. G. (2008). Structure and stability of nanogel particles prepared
455 by internal cross-linking of casein micelles. *International Dairy Journal*, 18(5), 556–565.
- 456 Jenness, R., & Koops, J. (1962). Preparation and properties of a salt solution which simulates
457 milk ultrafiltrate. *Netherlands Milk and Dairy Journal*, 16, 153–164.
- 458 Jaros, D., Jacob, M., Otto, C., & Rohm, H. (2010). Excessive cross-linking of caseins by
459 microbial transglutaminase and its impact on physical properties of acidified milk gels.
460 *International Dairy Journal*, 20(5), 321–327.
- 461 Jiao, Y., & Scha, T. E. (2004). Accurate height and volume measurements on soft samples
462 with the atomic force microscope. *Langmuir*, 20, 10038–10045.
- 463 Kasas, S., Longo, G., & Dietler, G. (2013). Mechanical properties of biological specimens

- 464 explored by atomic force microscopy. *Journal of Physics D-Applied Physics*, 46,
465 133001.
- 466 Katouzian, I., & Jafari, S.M. (2016). Nano-encapsulation as a promising approach for targeted
467 delivery and controlled release of vitamins. *Trends in Food Science & Technology*, 53,
468 34–48.
- 469 Lauber, S., Henle, T., & Klostermeyer, H. (2000). Relationship between the crosslinking of
470 caseins by transglutaminase and the gel strength of yoghurt. *European Food Research
471 and Technology*, 210, 305–309.
- 472 Livney, Y. D. (2010). Milk proteins as vehicles for bioactives. *Current Opinion in Colloid
473 and Interface Science*, 15(1–2), 73–83.
- 474 Lorenzen, P., Neve, H., Mautner, A., & Schlimme, E. (2002). Effect of enzymatic cross-
475 linking of milk proteins on functional properties of set-style yoghurt. *International
476 Journal of Dairy Technology*, 55(3), 152–157.
- 477 Marchin, S., Putaux, J. L., Pignon, F., & Léonil, J. (2007). Effects of the environmental
478 factors on the casein micelle structure studied by cryo transmission electron microscopy
479 and small-angle x-ray scattering/ultras-small-angle x-ray scattering. *Journal of Chemical
480 Physics*, 126(4), 045101.
- 481 Martin, M., Benzina, O., Szabo, V., Végh, A. G., Lucas, O., Cloitre, T., Scamps, F., &
482 Gergely, C. (2013). Morphology and nanomechanics of sensory neurons growth cones
483 following peripheral nerve injury. *Plos One*, 8(2), 1–11.
- 484 Martin, A. H., Goff, D. H., Smith, A., & Dalgleish, D. G. (2006). Immobilization of casein
485 micelles for probing their structure and interactions with polysaccharides using scanning
486 electron microscopy (SEM). *Food Hydrocolloids*, 20(6), 817–824.
- 487 McMahon, D. J., & Brown, R. J. (1984). Composition, structure, and integrity of casein
488 micelles: a review. *Journal of Dairy Science*, 67, 499-512.

- 489 McMahon, D. J., & Oommen, B. S. (2008). Supramolecular structure of the casein micelle.
490 *Journal of Dairy Science*, 91(5), 1709–1721.
- 491 Motoki, M., Seguro, K., Nio, N., & Takinami, T. (1986). Glutamine-specific deamidation of
492 α s1-casein by transglutaminase. *Agricultural and Biological Chemistry*, 50(12), 3025–
493 3030.
- 494 Nieuwland, M., Bouwman, W. G., Bennink, M. L., Silletti, E., & de Jongh, H. H. J. (2015).
495 Characterizing length scales that determine the mechanical behavior of gels from
496 crosslinked casein micelles. *Food Biophysics*, 10, 416-427.
- 497 Nogueira Silva, N. F., Bahri, A., Guyomarc'h, F., Beaucher, E., & Gaucheron, F. (2015).
498 AFM study of casein micelles cross-linked by genepin: effects of acid pH and citrate.
499 *Dairy Science and Technology*, 95(1), 75–86.
- 500 O'Sullivan, M. M., Kelly, A. L., & Fox, P. F. (2002). Effect of transglutaminase on the heat
501 stability of milk: A possible mechanism. *Journal of Dairy Science*, 85(1), 1–7.
- 502 Ouanezar, M., Guyomarc'h, F., & Bouchoux, A. (2012). AFM imaging of milk casein
503 micelles: evidence for structural rearrangement upon acidification. *Langmuir*, 28, 4915–
504 4919.
- 505 Prakash, V., & van Boekel, M. A. J. S. (2010). Nutraceuticals: possible future ingredients and
506 food safety aspects. In C. E. Boisrobert, A. Sjepanovic, S. Oh, & H. L. M. Lelieveld
507 (Eds.), *Ensuring Global Food Safety* (pp. 333–338). Oxford: University Press.
- 508 Ranadheera, C. S., Liyanaarachchi, W. S., Chandrapala, J., Dissanayake, M., & Vasiljevic, T.
509 (2016). Utilizing unique properties of caseins and the casein micelle for delivery of
510 sensitive food ingredients and bioactives. *Trends in Food Science and Technology*, 57,
511 178–187.
- 512 Regnault, S., Thiebaud, M., Dumay, E., & Cheftel, J. C. (2004). Pressurisation of raw skim
513 milk and of a dispersion of phosphocaseinate at 9 °C or 20 °C: Effects on casein micelle

- 514 size distribution. *International Dairy Journal*, 14(1), 55–68.
- 515 Romeih, E., & Walker, G. (2017). Recent advances on microbial transglutaminase and dairy
516 application. *Trends in Food Science and Technology*, 62, 133–140.
- 517 Rosenbluth, M. J., Lam, W. A., & Fletcher, D. A. (2006). Force microscopy of nonadherent
518 cells : A comparison of leukemia cell deformability, 90(1762), 2994–3003.
- 519 Russel, S. (2009). *Contact Angle Measurement Technique for Rough Surfaces*. Michigan
520 Technological University.
- 521 Sharma, R., Lorenzen, P. C., & Qvist, K. B. (2001). Influence of transglutaminase treatment
522 of skim milk on the formation of ϵ -(-glutamyl)lysine and the susceptibility of individual
523 proteins towards crosslinking. *International Dairy Journal*, 11(10), 785–793.
- 524 Smiddy, M. A., Martin, J.E. G. H., Kelly, A. L., de Kruif, C. G., & Huppertz, T. (2006).
525 Stability of casein micelles cross-linked by transglutaminase. *Journal of Dairy Science*,
526 89(6), 1906–14.
- 527 Uricanu, V. I., Duits, M. H. G., & Mellema, J. (2004). Hierarchical networks of casein
528 proteins: An elasticity study based on atomic force microscopy. *Langmuir*, 20(12),
529 5079–5090.
- 530 Walstra, P., Geurts, T. J., Noomen, A., Jellema, A., & van Boekel, M. A. J. S. (1999). Milk
531 components. In P. Walstra, T. J. Geurts, A. Noomen, A. Jellema, & M. A. J. S. van
532 Boekel (Eds.), *Dairy Technology* (pp. 27–105). New York: Marcel Dekker.
- 533 Yokoyama, K., Nio, N., & Kikuchi, Y. (2004). Properties and applications of microbial
534 transglutaminase. *Applied Microbiology and Biotechnology*, 64(4), 447–454.
- 535 Yuehua, Y., & Randall, L. (2013). Surface science techniques. In *Springer Series in Surface*
536 *Sciences* (Vol. 51, pp. 3–34).
- 537 Zhu, F. (2017). Encapsulation and delivery of food ingredients using starch based systems.
538 *Food Chemistry*, 229, 542–552.

539 **Figure captions**

540 **Figure 1:** Native CM (a, b, e, f, i, j) and transglutaminase cross-linked CM (c, d, g, h, k, l)
541 topography. AFM height (a, c, e, g) and deflection (b, d, f, h) images, height profile (i, k) at
542 the selected black scan line on (e, g), three-dimensional AFM height image (j, l) of CM and
543 TG-CM CM. CM and TG-CM were captured on SAM via MAH-PSer/Thr/Tyr antibody.
544 Images were performed in liquid (SMUF, pH 6.6) in contact mode. The white scale bar (a-h)
545 represents 1 μm . The colored scale bar (a, c, e, g) represents the height range between 0 and
546 120 nm. The grey scale bar (b, d, f, h) represents the deflection range between 0 and 30 nm.

547
548 **Figure 2:** SEM images of native CM (a, c) and transglutaminase cross-linked CM (b, d) on
549 ANODISC® membrane at two different magnifications.

550
551 **Figure 3:** Particle size distribution curves of native (■) and TG cross-linked (●) CM (5%,
552 w/w) determined by photon correlation spectroscopy (PCS) in light intensity. PCS
553 measurements were carried out at 25 °C. Mean curves from six PCS determinations are
554 shown.

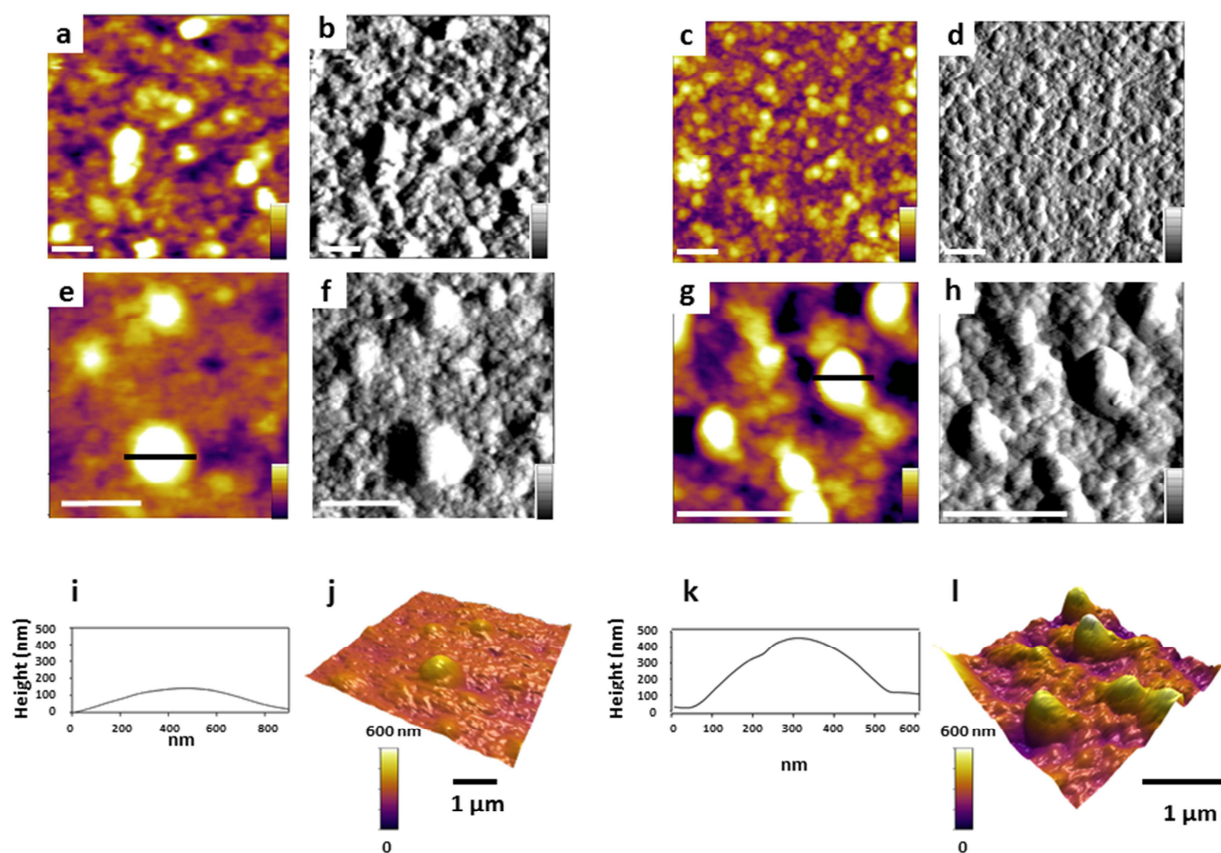
555
556 **Figure 4:** Histograms of width (a) and height (b) and height versus width plots (c-d) for TG
557 cross-linked (a, b, c) and native (d) CM. Height and width histograms were best fitted with a
558 Gaussian function. The dotted lines in the height vs width plots show the linear ratio between
559 width and height of a perfectly spherical particles.

560
561 **Figure 5:** AFM elasticity distribution indicating the stiffness of TG-CM in a liquid native
562 environment (SMUF, pH 6.6). Young's modulus (E) distribution was best fitted with 3
563 Gaussian peaks centered at 218 ± 14 kPa, 536 ± 10 kPa and 711 ± 11 kPa (solid line).

564 Young's modulus distribution fit of native CM is proposed (dotted line) centered at 269 ± 14
565 kPa. 10 loading forces were applied on 20 different CM in order to obtain 200 analyzed
566 curves.

ACCEPTED MANUSCRIPT

Figure 1



Comment citer ce document :

Bahri, A., Martin, M., Gergely, Marchesseau, S., Chevalier-Lucia, D. (2018). Topographical and nanomechanical characterization of casein nanogel particles using atomic force microscopy. *Food Hydrocolloids*, 83, 53-60. , DOI : 10.1016/j.foodhyd.2018.03.029

Figure 2

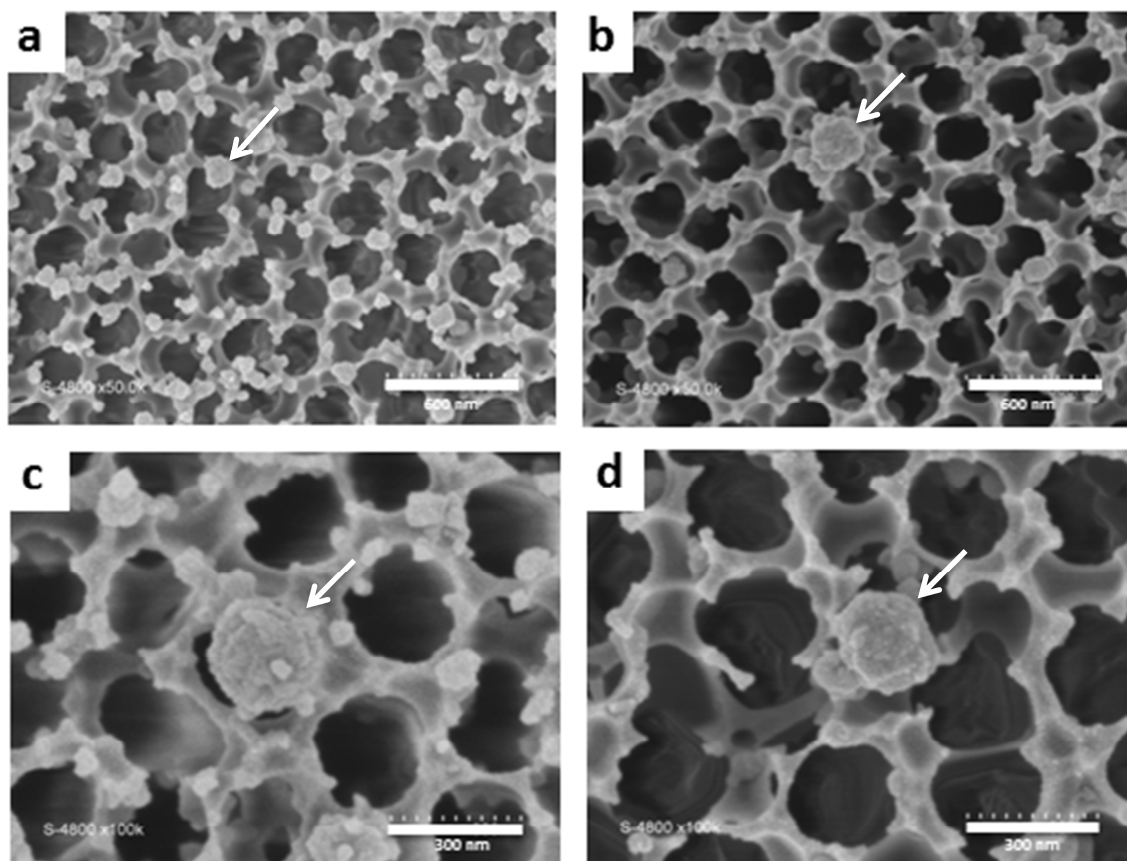
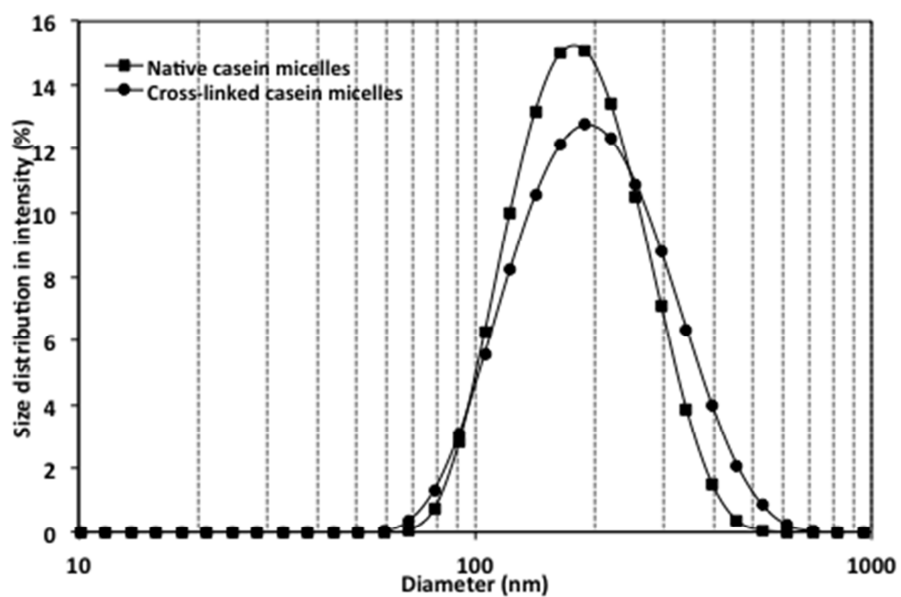


Figure 3



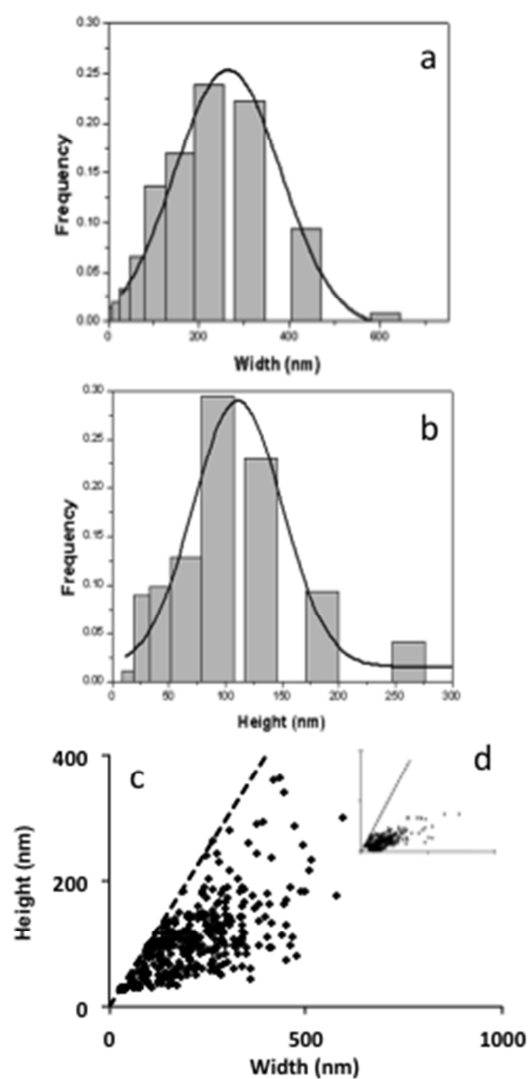
APT

ACCEPTED MANUSCRIPT

Comment citer ce document :

Bahri, A., Martin, M., Gergely, Marchesseau, S., Chevalier-Lucia, D. (2018). Topographical and nanomechanical characterization of casein nanogel particles using atomic force microscopy. Food Hydrocolloids, 83, 53-60. , DOI : 10.1016/j.foodhyd.2018.03.029

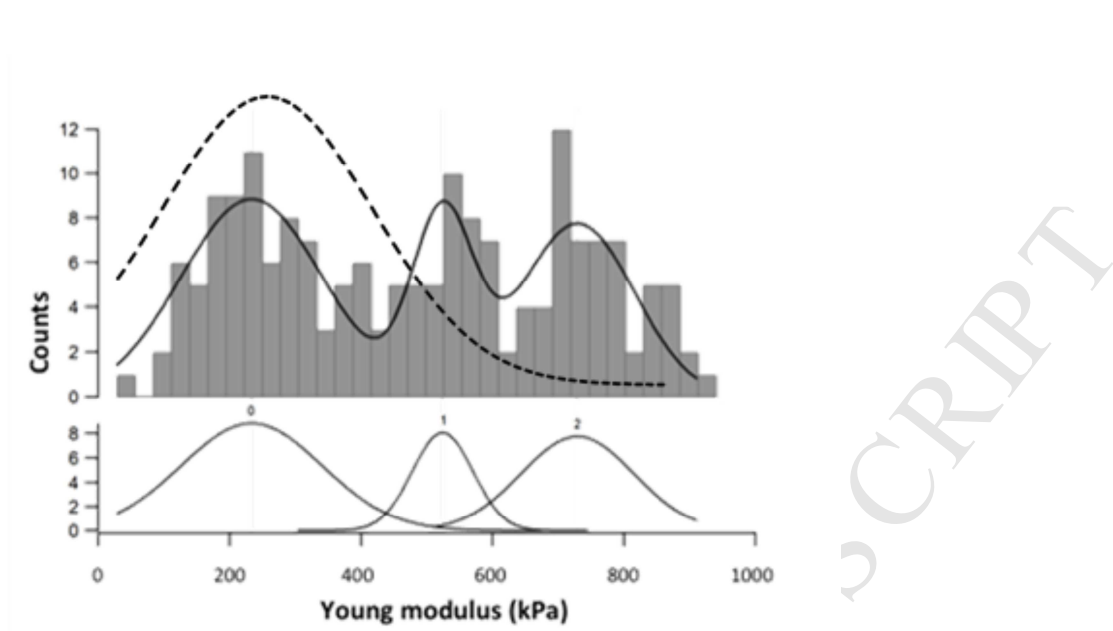
Figure 4



Comment citer ce document :

Bahri, A., Martin, M., Gergely, Marchesseau, S., Chevalier-Lucia, D. (2018). Topographical and nanomechanical characterization of casein nanogel particles using atomic force microscopy. Food Hydrocolloids, 83, 53-60. , DOI : 10.1016/j.foodhyd.2018.03.029

Figure 5



Highlights

- TG cross-linked CM topography and nanomechanics were evaluated by AFM in liquid.
- TG cross-linked CM are significantly wider and higher than native CM.
- TG-CM are less flattened once captured on gold substrate compared to native CM.
- TG-CM stiffness distribution is multimodal with stiffer peaks compared to native CM.

ACCEPTED MANUSCRIPT

Comment citer ce document :

Bahri, A., Martin, M., Gergely, Marchesseau, S., Chevalier-Lucia, D. (2018). Topographical and nanomechanical characterization of casein nanogel particles using atomic force microscopy. *Food Hydrocolloids*, 83, 53-60. , DOI : 10.1016/j.foodhyd.2018.03.029